10162 *Biochemistry* **2009,** *48,* 10162–10174
DOI: 10.1021/bi900939w

BIOCHEMISTRY
including biophysical chemistry & molecular biology
Article

Characterization of RimO, a New Member of the Methylthiotransferase Subclass of the Radical SAM Superfamily[†]

Kyung-Hoon Lee,[‡,@] Lana Saleh,*[,∥,@] Brian P. Anton,[⊥,∥] Catherine L. Madinger,[∥] Jack S. Benner,[∥] David F. Iwig,[§] Richard J. Roberts,[∥] Carsten Krebs,*[,‡,§] and Squire J. Booker*[,‡,§]

[‡]*Department of Chemistry and* [§]*Department of Biochemistry and Molecular Biology, The Pennsylvania State University, University Park, Pennsylvania 16802,* [∥]*New England Biolabs, Ipswich, Massachusetts 01938, and* [⊥]*Bioinformatics Program, Boston University, Boston, Massachusetts 02215* [@]*These authors contributed equally to this work.*

Received June 3, 2009; Revised Manuscript Received September 8, 2009

ABSTRACT: RimO, encoded by the *yliG* gene in *Escherichia coli*, has been recently identified in vivo as the enzyme responsible for the attachment of a methylthio group on the β-carbon of Asp88 of the small ribosomal protein S12 [Anton, B. P., Saleh, L., Benner, J. S., Raleigh, E. A., Kasif, S., and Roberts, R. J. (2008) *Proc. Natl. Acad. Sci. U.S.A. 105*, 1826−1831]. To date, it is the only enzyme known to catalyze methylthiolation of a protein substrate; the four other naturally occurring methylthio modifications have been observed on tRNA. All members of the methylthiotransferase (MTTase) family, to which RimO belongs, have been shown to contain the canonical CxxxCxxC motif in their primary structures that is typical of the radical *S*-adenosylmethionine (SAM) family of proteins. MiaB, the only characterized MTTase, and the enzyme experimentally shown to be responsible for methylthiolation of N^6-isopentenyladenosine of tRNA in *E. coli* and *Thermotoga maritima*, has been demonstrated to harbor two distinct [4Fe-4S] clusters. Herein, we report in vitro biochemical and spectroscopic characterization of RimO. We show by analytical and spectroscopic methods that RimO, overproduced in *E. coli* in the presence of iron−sulfur cluster biosynthesis proteins from *Azotobacter vinelandii*, contains one $[4Fe\text{-}4S]^{2+}$ cluster. Reconstitution of this form of RimO ($RimO_{rcn}$) with ^{57}Fe and sodium sulfide results in a protein that contains two $[4Fe\text{-}4S]^{2+}$ clusters, similar to MiaB. We also show by mass spectrometry that $RimO_{rcn}$ catalyzes the attachment of a methylthio group to a peptide substrate analogue that mimics the loop structure bearing aspartyl 88 of the S12 ribosomal protein from *E. coli*. Kinetic analysis of this reaction shows that the activity of $RimO_{rcn}$ in the presence of the substrate analogue does not support a complete turnover. We discuss the possible requirement for an assembled ribosome for fully active RimO in vitro. Our findings are consistent with those of other enzymes that catalyze sulfur insertion, such as biotin synthase, lipoyl synthase, and MiaB.

It has been known for some time that ribosomal protein S12 undergoes a unique post-translational modification, methylthiolation of the β-carbon of residue D88 in *Escherichia coli* and several other bacteria (*1*). Interestingly, this residue is strictly conserved in all known S12 homologues—although the modification is not—and is located near the functional center of the ribosome (*1*, *2*). RimO, the *yliG* gene product, has been recently identified as the enzyme responsible for this modification in *E. coli* (Scheme 1) (*3*). RimO bears strong sequence similarity to the product of the *miaB* gene, which has been shown to catalyze the methylthiolation of C^2 of N^6-isopentenyladenosine (i^6A)[1] of tRNA in *E. coli* and *Thermotoga maritima* to form 2-methylthio-N^6-isopentenyladenosine (ms^2i^6A) (*4*−*6*). Using phylogenomic analysis and existing tRNA modification data, RimO and

[†]This work was supported by National Institutes of Health Grant GM-63847 and National Science Foundation Grant MCB-0133826 (S.J.B.), the Dreyfus Foundation (Teacher Scholar Award to C.K.), the Beckman Foundation (Young Investigator Award to C.K.), and New England Biolabs.

*To whom correspondence should be addressed. S.J.B.: 104 Chemistry Building, The Pennsylvania State University, University Park, PA 16802; phone, (814) 865-8793; fax, (814) 865-2927; e-mail, squire@psu.edu. C.K.: 104 Chemistry Building, The Pennsylvania State University, University Park, PA 16802; phone, (814) 865-6089; fax, (814) 865-2927; e-mail, ckrebs@psu.edu. L.S.: 240 County Road, Ipswich, MA 01908; phone, (978) 380-7446; fax, (978) 921-1350; e-mail, saleh@neb.com.

[1]Abbreviations: AI, as-isolated; BS, biotin synthase; BSA, bovine serum albumin; 5′-dA, 5′-deoxyadenosine; 5′-dA$^{\bullet}$, 5′-deoxyadenosyl 5′-radical; DTT, dithiothreitol; EDTA, ethylenediaminetetraacetic acid; EPR, electron paramagnetic resonance; ESI-TOF MS, electrospray ionization time-of-flight mass spectrometry; ESI-MS/MS, electrospray ionization tandem mass spectrometry; Fe−S, iron−sulfur; HEPES, *N*-(2-hydroxyethyl)piperazine-*N*′-2-ethanesulfonic acid; HPLC, high-performance liquid chromatography; i^6A, N^6-isopentenyladenosine; ms^2i^6A, 2-methylthio-N^6-isopentenyladenosine; MALDI-TOF MS, matrix-assisted laser desorption ionization time-of-flight mass spectrometry; MTase, methyltransferase; MTTase, methylthiotransferase; IMAC, immobilized metal affinity chromatography; IPTG, isopropyl β-D-thiogalactopyranoside; IS, internal standard; LB, Luria-Bertani; LS, lipoyl synthase; MW, molecular weight; Ni-NTA, nickel nitrilotriacetic acid; PCR, polymerase chain reaction; PFL-AE, pyruvate formate-lyase activating enzyme; RCN, reconstituted; $RimO_{ai}$, as-isolated $RimO_H$; $RimO_H$, His-tagged RimO; $RimO_{rcn}$, reconstituted $RimO_H$; RS, radical SAM; SAH, *S*-adenosyl-L-homocysteine; SAM, *S*-adenosyl-L-methionine; SDS−PAGE, sodium dodecyl sulfate−polyacrylamide gel electrophoresis; TRAM, TRM2 and MiaB; UV−vis, ultraviolet−visible; WT, wild-type.

 Published on Web 09/08/2009

Table 1: Four Clades of the MTTase Family

	origin of members	representative members	substrate	product
RimO	bacterial	*E. coli*, *Rhodopseudomonas palustris*, *Thermus thermophilus*	S12	β-methylthio-D88
MiaB	bacterial and mitochondrial	*E. coli*, *T. maritima*	tRNA	ms^2i^6A
YqeV[c]	bacterial	*Bacillus subtilis*	tRNA	ms^2t^6A[a] ms^2hn^6A[b]
Mj0867[c]	archaeal and eukaryotic	*Methanocaldococcus jannaschii*	tRNA	ms^2t^6A ms^2hn^6A

[a] ms^2t^6A, 2-methylthio-N^6-threonylcarbamoyladenosine. [b] ms^2hn^6A, 2-methylthio-N^6-(hydroxynorvalyl)carbamoyladenosine. [c] Substrates and products are predicted only.

Scheme 1: Reaction Catalyzed by *E. coli* RimO, the Methylthiolation of Aspartyl 88 of Protein S12 of the Ribosome

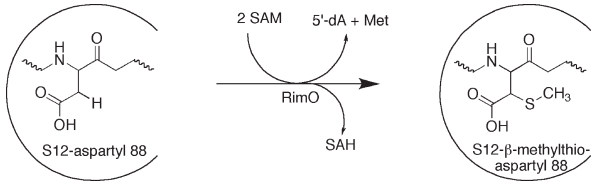

MiaB have been shown to be members of an ancient family of methylthiotransferases (MTTase) (*3*). This family is divided into four subgroups, three of which are involved in the methylthiolation of tRNA—or are presumed to be so—while the fourth, to which RimO belongs, is potentially unique in its modification of protein (Table 1). Despite this difference in the nature of the substrate modified, RimO has not significantly diverged from the other three subgroups at the level of primary structure. All known MTTases share three major domains: an N-terminal domain, UPF0004 (uncharacterized protein family 0004), which contains three conserved cysteines thought to ligate an iron−sulfur (Fe−S) cluster responsible for sulfur mobilization and insertion into the substrate; a central radical *S*-adenosylmethionine (SAM) domain containing the canonical CxxxCxxC motif; and a C-terminal TRAM (TRM2 and MiaB) domain, presumed to be responsible for substrate recognition (*3*, *7*).

The presence of a TRAM domain in RimO is intriguing considering that it is typically found in tRNA-modifying enzymes, namely, uridine methyltransferases of the TRM2 family and enzymes of the MiaB family, and has been shown to be involved in binding the RNA substrate, as observed in *E. coli* RumA (*8*−*10*). Since the substrate for RimO is ribosomal protein S12 and not tRNA, either the S12 loop containing D88 is structurally similar to tRNA and is thus recognized by the TRAM domain (precedent is set by certain protein translation factors that are believed to resemble tRNA) (*11*, *12*) or the TRAM domain binds an RNA stem-loop proximal to, or in contact with, S12 in the assembled ribosome. The crystal structure of S12 from *Thermus thermophilus* shows that the modified residue, D88, resides on a conserved loop that extends toward the acceptor site of the ribosome (*2*). Moreover, this residue is in close contact with the 530 stem-loop of 16S rRNA, specifically nucleotides 525, 526, 911−914, and 1491 (*3*, *13*, *14*). These two scenarios should be distinguishable experimentally, because free S12 is the substrate in the first scenario, while the ribosome has to be assembled for RimO to perform its catalytic function on S12 in the second.

The identification of RimO as a potential MTTase has yet added to the list of radical SAM (RS) enzymes involved in sulfur insertion (*15*). Biotin synthase (BS), lipoyl synthase (LS), and MiaB are all members of this special class of RS enzymes. BS catalyzes the insertion of one sulfur atom between carbons 6 and 9 of dethiobiotin, resulting in the formation of a thiophane ring (*16*); LS catalyzes the insertion of two sulfur atoms into two different C−H bonds at carbons 6 and 8 of an octanoyl fatty acyl chain bound covalently to a protein lysyl residue, resulting in the generation of the lipoyl cofactor (*17*−*19*), and MiaB catalyzes methylthiolation of the aromatic C^2−H bond of N^6-isopentenyladenosine (i^6A) of tRNA to form ms^2i^6A (*20*). The activation of these highly unreactive C−H bonds for sulfur insertion is performed by a 5′-deoxyadenosyl 5′-radical (5′-dA•), a strong oxidizing agent, which is produced via reductive cleavage of SAM. A reduced Fe−S cluster, $[4Fe\text{-}4S]^+$, coordinated by three cysteinyl residues housed in a conserved CxxxCxxC motif, provides the requisite electron. In each of these proteins, a second Fe−S cluster has been uncovered. This second cluster, a [4Fe-4S] cluster in both LS and MiaB (*21*, *22*) and a [2Fe-2S] cluster in BS (*23*−*25*), is thought to be the source of the incorporated sulfur atom.

In addition to thiolation of residue D88 of protein S12, it has been suggested that RimO performs methylation on the presumed thiol-containing intermediate, although the possibility of the involvement of a second unidentified protein could not be excluded (*3*). MiaB, the only characterized MTTase, has been shown to catalyze both thiolation and methylation of i^6A (*20*). The level of similarity in sequence and domain structure between RimO and MiaB suggests that RimO is also responsible for both reactions in the D88 modification and implies that 2 equiv of SAM must be expended per modification generated: one to generate the 5′-dA• to initiate catalysis and one to methylate the β-thioaspartyl intermediate, resulting in release of *S*-adenosyl-L-homocysteine (SAH) (Scheme 1).

In this work, we demonstrate experimentally that RimO is indeed a member of the special class of RS proteins that catalyze insertion of sulfur into unactivated C−H bonds. As such, we show that it contains two spectroscopically distinguishable [4Fe-4S] clusters: one that is ligated by cysteines 150, 154, and 157, residing in the CxxxCxxC motif, strictly conserved among the overwhelming majority of RS proteins; and one that is ligated presumably by cysteines 17, 53, and 82, which are conserved among RimO homologues. In addition, we demonstrate that the fully reconstituted protein is capable of catalyzing methylthiolation in the presence of a peptide analogue of the S12 loop containing D88.

MATERIALS AND METHODS

Materials. All DNA-modifying enzymes and reagents, as well as the T7 Express overproducing strain, were from New England Biolabs (Ipswich, MA). Expression vector pET-28c was purchased from Novagen (Madison, WI). Sodium sulfide (nonahydrate),

L-tryptophan, 2-mercaptoethanol, L-(+)-arabinose, ferric chloride, 5′-deoxyadenosine (5′-dA), and SAH were purchased from Sigma Corp. (St. Louis, MO). *N*-(2-Hydroxyethyl)piperazine-*N*′-2-ethanesulfonic acid (HEPES) was purchased from Fisher Scientific (Pittsburgh, PA), and imidazole was purchased from J. T. Baker Chemical Co. (Phillipsburg, NJ). Potassium chloride and glycerol were purchased from EMD Chemicals (Gibbstown, NJ), while dithiothreitol (DTT) was purchased from Gold Biotechnology (St. Louis, MO). Coomassie blue dye binding reagent for protein concentration determination was purchased from Pierce (Rockford, IL), as was the bovine serum albumin standard (2 mg/mL). Nick prepoured gel-filtration columns and Sephadex G-25 resin were purchased from GE Biosciences (Piscataway, NJ), while nickel nitrilotriacetic acid (Ni-NTA) resin was purchased from Qiagen (Valencia, CA). All other buffers and chemicals were of the highest grade available.

SAM and *S*-adenosyl-L-[*methyl*-d_3]methionine were synthesized and purified as described previously (*26*). Recombinant *E. coli* flavodoxin (Flv) and flavodoxin reductase (Flx) were purified from *E. coli*-harboring plasmids containing each of the relevant genes cloned into intein-based expression vector pTYB1 (New England Biolabs). Purification was conducted by affinity chromatography, and the isolated proteins contained no amino acids that were not encoded by the natural gene sequence (*17*).

^{57}Fe (97−98%) metal, used in Mössbauer spectroscopy, was purchased from Isoflex USA (San Francisco, CA). For preparation of a $^{57}FeSO_4$ solution, the solid was washed with $CHCl_3$ and dissolved with heating in an anaerobic solution of 2 N H_2SO_4 (1.5 mol of H_2SO_4/mol of ^{57}Fe). SPEX (Metuchen, NJ) CertiPrep Cläritas PPT single-element Fe (1000 mg/L in 2% HNO_3) was used to prepare iron standards for quantitative iron analysis.

The peptide substrate, **P1** (NH_2-RGGRVK**D**LPGVRY-COOH), was synthesized by the Peptide Synthesis Facility at New England Biolabs. The sequence of the peptide corresponds to residues 83−95 of the *E. coli* S12 protein. The Asp residue (**D**) in bold type corresponds to D88, the site of modification by RimO. The synthesized peptide was characterized as the desired product by electrospray ionization tandem mass spectrometry (ESI-MS/MS) using a 6330 ion trap mass spectrometer with nano-electrospray ionization (Agilent Technologies, Santa Clara, CA). An RNA oligonucleotide (5′-AAG-CAC-CGG-CUA-ACU-CCG-UGC-CAG-CAG-CCG-CGG-UAA-UAC-GGA-GGG-UGC AA-3′) corresponding to bases 498−547 of *E. coli* 16S rRNA was synthesized by the Oligonucleotide Synthesis Facility at New England Biolabs.

UV−visible spectra were recorded on a Cary 50 spectrometer from Varian (Walnut Creek, CA) using the WinUV software package for spectral manipulation and to control the instrument. Oxygen-sensitive samples were prepared in an anaerobic chamber and aliquoted into cuvettes that were sealed before removal from the chamber. High-performance liquid chromatography (HPLC) was conducted on an Agilent Technologies 1100 system that contained a variable-wavelength detector and an autosampler for sample injection. The instrument was operated via the ChemStation software package, which was also used for data analysis. Sonic disruption of *E. coli* cell suspensions was conducted with a 550 sonic dismembrator from Fisher Scientific using a horn containing a 1/2 in. tip. The cable was threaded through a port in a Coy (Grass Lakes, MI) anaerobic chamber to allow the process to be performed anoxically.

Overexpression of the yliG Gene. Construction of plasmid pET28-yliG, the overexpression vector for the *yliG* gene, has been described previously (*3*). Production of hexahistidine-tagged RimO ($RimO_H$) from a T7 Express overproducing strain (New England Biolabs) carrying plasmids pET28-yliG (*3*) and pDB1282 was conducted according to the previously described procedure for LS (*17*). A yield of 2.5 g of wet cell paste per liter of culture was obtained.

Purification of RimO$_H$. Purification of $RimO_H$ was conducted by immobilized metal affinity chromatography (IMAC) using Ni-NTA resin according to the previously described procedure for LS (*17*). All of the purification steps were performed in a Coy anaerobic chamber, which was kept under an atmosphere of N_2 and H_2 (95%/5%); the O_2 concentration was maintained below 1 ppm via the use of palladium catalysts. Precautionary steps taken to maintain anaerobic conditions throughout the purification procedure were as described previously (*17*, *21*). Buffers used during the purification were as follows: lysis buffer [50 mM HEPES (pH 7.5), 300 mM KCl, 10 mM 2-mercaptoethanol, 20 mM imidazole, and 1 mg/mL lysozyme], wash buffer [50 mM HEPES (pH 7.5), 300 mM KCl, 10 mM 2-mercaptoethanol, 10% (v/v) glycerol, and 40 mM imidazole], and elution buffer (wash buffer containing 250 mM imidazole). Fractions containing $RimO_H$, distinguished by their dark brown color, were pooled and concentrated in an Amicon ultrafiltration cell (Millipore, Billerica, MA) fitted with a YM30 membrane (30,000 MW cutoff). The protein was exchanged into storage buffer [50 mM HEPES (pH 7.5), 300 mM KCl, 20% glycerol, and 1 mM DTT] using a Sephadex G25 column (2.5 cm × 13 cm), reconcentrated, and stored in aliquots in a liquid N_2 dewar until the protein was ready for use.

Protein, Iron, and Sulfide Quantification. The concentration of $RimO_H$ was determined by the procedure of Bradford (*27*). Quantitative amino acid analysis on as-isolated $RimO_H$ ($RimO_{ai}$) was performed at the Molecular Biology Core Facility of the Dana Farber Institute (Boston, MA). A yield of ∼3.5 mg of protein/g of cell paste was obtained from the procedure described above. Iron and sulfide analyses were performed according to the procedures of Beinert (*28*−*30*).

Chemical Reconstitution of RimO$_{ai}$ with Iron and Sulfide. Chemical reconstitution of $RimO_{ai}$ was conducted on ice and under anaerobic conditions. The protein was treated with 10 mM DTT before it was incubated for 10 min with an 8-fold molar excess of $FeCl_3$ or $^{57}FeSO_4$. An 8-fold molar excess of sodium sulfide was added over the course of 3−4 h, and then the solution was subjected to centrifugation at 18,000*g*. The supernatant was exchanged into storage buffer by gel filtration (G25) chromatography and concentrated by ultrafiltration using an Amicon stirred cell fitted with a YM10 membrane.

Electron Paramagnetic Resonance (EPR) Spectroscopy. Preparation of protein samples for EPR analysis was as previously described (*21*). X-Band (∼9.5 GHz) EPR spectra were acquired on a Bruker ESP 300 spectrometer equipped with an Oxford Instruments model ESP 900 continuous-flow cryostat. Samples were loaded into EPR tubes (2 mm inside diameter) inside the anaerobic chamber, sealed with a septum, and then flash-frozen in liquid N_2. Experimental details and EPR parameters for the different samples are given in the figure legends.

Mössbauer Spectroscopy. The preparation of samples for Mössbauer analysis has been described previously (*21*).

Mössbauer spectra were recorded on spectrometers from WEB Research (Edina, MN) operating in constant acceleration mode in transmission geometry. For collection of low-field spectra, the sample was kept inside a SVT-400 dewar from Janis (Wilmington, MA) at a temperature of 4.2 K and in a magnetic field of 53 mT applied parallel to the γ-beam. For high-field spectra, the sample was kept inside a 12SVT dewar (Janis), which houses a superconducting magnet that allows for application of variable magnetic fields between 0 and 8 T parallel to the γ-beam. The isomer shifts quoted are relative to the centroid of the spectrum of a metallic foil of α-Fe at room temperature. Data analysis was performed using WMOSS from WEB Research.

RimO Activity Assay. The time-dependent formation of 5′-dA and SAH was determined from the same reaction mixtures, which contained the following in a volume of 400 μL: 100 μM reconstituted RimO ($RimO_{rcn}$), 700 μM SAM, 300 μM peptide substrate, 50 mM Na-HEPES (pH 7.5), 2 mM dithionite, and 1 mM tryptophan, used as an internal standard (IS). When the RNA oligonucleotide was used, it was added to the reaction mixture at a final concentration of 175 μM. All components except SAM were incubated at 37 °C for 3 min before the reaction was initiated with the omitted component. Aliquots (25 μL) of the reaction mixture were withdrawn at various times from 0 to 180 min and added to 25 μL of 0.1 N H_2SO_4 to quench the reaction. Precipitated protein was removed by centrifugation at 18,000*g* for 15 min, and a 20 μL aliquot of the resulting supernatant was subjected to analysis by HPLC using a Zorbax SB-CN column (4.6 mm × 250 mm, 5 μm) from Agilent Technologies. Solvent A consisted of 0.4% trifluoroacetic acid (TFA) titrated to pH 1.8 with triethylamine (TEA), while solvents B and C consisted of 100% acetonitrile and 100% methanol, respectively. The column was equilibrated in 95% solvent A and 5% solvent C at a flow rate of 1 mL/min, and the UV−vis detector was set to monitor at 260 nm. After sample injection, the conditions described above were maintained for 5 min before simultaneous linear gradients from 0 to 5% solvent B and 5 to 30% solvent C were applied over 10 min. Under these conditions, SAM eluted at 3.1 min, adenine eluted at 4.5 min, SAH eluted at 5.9 min, 5′-dA eluted at 6.6 min, methylthioadenosine eluted at 11.1 min, and the tryptophan IS eluted at 12.7 min. Calibration curves of known concentrations of 5′-dA and SAH, run under identical conditions, were used to quantify their concentrations generated in the assay, while the IS facilitated accurate quantification from sample to sample.

Mass Spectrometry. Peptides were enriched from the quenched assay mixtures, described in the previous section, using pipet $ZipTips_{C18}$ (Millipore) according to the manufacturer's instructions. Peptides were eluted with a 50:50 solution of acetonitrile and 0.1% formic acid in water, dried to completion under vacuum, and resuspended in 20 μL of 0.1% formic acid. Samples (8 μL) were injected into an HPLC-Chip Cube system and separated on a Protein ID chip comprised of a 40 nL enrichment column, a 75 μm × 150 mm separation column packed with Zorbax 300SB-C18 5 μm material, and a spray emitter with a 15 μm flow path (Agilent Technologies). Peptides were separated using a 40 min 5 to 45% B linear gradient (A being 0.1% formic acid and B being acetonitrile and 0.1% formic acid) at a flow rate of 0.4 μL/min and analyzed online using a 6330 ion trap mass spectrometer with nanoelectrospray ionization (Agilent Technologies). A capillary voltage of 1,700−1,900 V (optimized on a per chip basis) was used, and the skimmer voltage was held at 30 V. Data were acquired at 25,000 m/z s^{-1} with a SmartTarget value of 500,000 and maximum accumulation time of 200 ms. The mass spectrum acquisition range was from m/z 300 to 1,800. Default parameters for Auto MS^2 were used. Ions were selected for fragmentation on the basis of their intensity, with the number of precursor ions set to five. The MS/MS fragmentation amplitude was set to 1.30 V with SmartFrag start and end amplitude values set to 30 and 200%, respectively. The MS/MS acquisition range was from m/z 50 to 2,200. Data acquisition was coordinated with the start of the LC separation and was stopped after 60 min. The ESI-MS/MS data were then analyzed to determine the point of SCH_3 modification. Analysis of the modification by matrix-assisted laser desorption ionization time-of-flight mass spectrometry (MALDI-TOF MS) was conducted at the Proteomics and Mass Spectrometry Core Facility at the Pennsylvania State University as described previously (*31*).

RESULTS

Expression of the E. coli yliG Gene and Purification of Its Protein Product, $RimO_H$. The primary structure of RimO contains a CxxxCxxC motif, which has become a signature sequence for proteins in the RS superfamily (*32*). The cysteines in this motif coordinate an O_2-sensitive [4Fe-4S] cluster that is required for turnover (*33*−*36*). To facilitate the production of significant amounts of soluble and active $RimO_H$, the *E. coli yliG* gene was coexpressed with genes from an *Azotobacter vinelandii* operon, harbored on plasmid pDB1282, that encode protein products (IscS, IscU, IscA, HscB, HscA, and Fdx) that are known to be involved in Fe−S cluster biosynthesis (*17*, *37*) (Figure S1 of the Supporting Information). Cells were cultured in M9 minimal medium under semianaerobic conditions and in the presence of ^{57}Fe to facilitate analysis of the purified protein by Mössbauer spectroscopy. Purification of $RimO_H$ by IMAC under anaerobic conditions typically yielded 3−4 mg of protein per gram of wet cell paste. The protein displayed an apparent molecular mass of ~50 kDa, consistent with its known molecular mass of 49,582 Da as determined from its primary structure, and was estimated to be greater than 95% pure by denaturing polyacrylamide gel electrophoresis with Coomassie staining (Figure S2 of the Supporting Information). Quantitative amino acid analysis, employed to establish an extinction coefficient for $RimO_{ai}$ (i.e. as-isolated RimOH), showed that the Bradford assay, using BSA as a standard, overestimates the concentration of the protein by a factor of 1.84.

Spectroscopic and Analytical Characterization of $RimO_{ai}$. The UV−visible absorption spectrum of $RimO_{ai}$, shown in Figure 1 (solid line), displays a typical protein absorption peak at ~280 nm, a small absorption shoulder at ~320 nm, and a broad peak at ~410 nm with tailing that extends beyond 700 nm. The ratio of the absorbance at 280 nm to that at 410 nm (A_{280}/A_{410}), which provides a qualitative assessment of cluster content, is 4.2. These features, as well as the brown color of the protein, are consistent with the presence of Fe−S cluster(s). Analyses for the iron and sulfide content of $RimO_{ai}$ yielded 4.4 ± 0.2 equiv of the former and 3.9 ± 0.4 equiv of the latter per polypeptide (average and standard deviation of four independent determinations) using the Bradford correction factor for protein concentration determination.

The X-band EPR spectrum of $RimO_{ai}$ taken at 14 K (Figure 2A) shows an isotropic EPR signal centered at g = 2.01 with a line width of ~50 G. This signal corresponds to < 1% of spin per protein and therefore represents an only minor

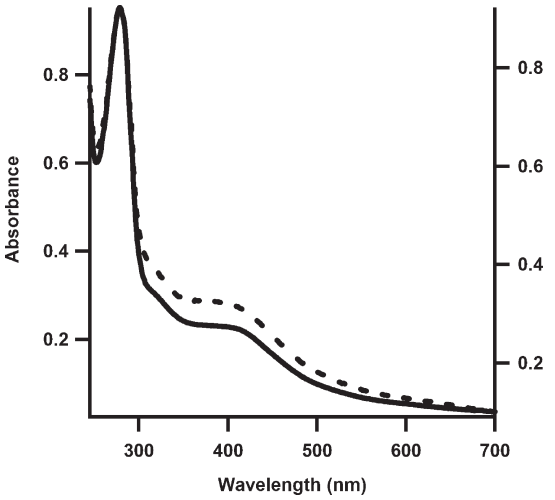

FIGURE 1: UV−visible spectra of $RimO_{ai}$ (solid line, left *Y*-axis) and $RimO_{rcn}$ (dashed line, right *Y*-axis). Sample concentrations were 9.5 μM for $RimO_{ai}$ and 5.5 μM for $RimO_{rcn}$. A_{280}/A_{410} ratios were 4.2 and 2.9 for $RimO_{ai}$ and $RimO_{rcn}$, respectively.

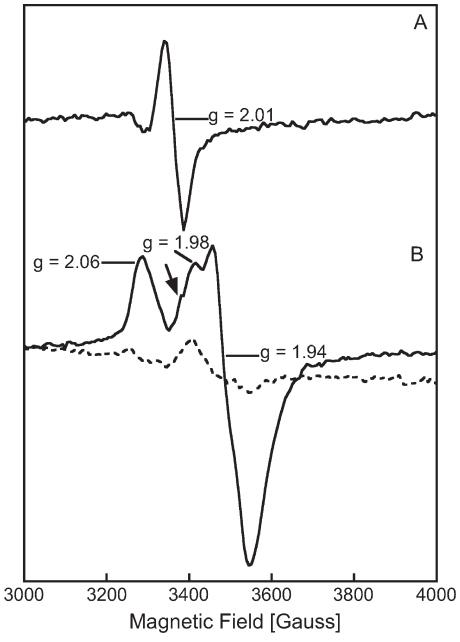

FIGURE 2: X-Band EPR spectra of (A) $RimO_{ai}$ and (B) $RimO_{ai}$ reduced with sodium dithionite. The solid line spectra in panels A and B were recorded at a temperature of 14 K, while the dashed line spectrum in panel B was recorded at a temperature of 64 K. The arrow in spectrum (B, solid line) is pointing to a $g = 2.0$ signal resulting from a cavity contaminant. In both panels, the concentration of the protein sample was 0.45 mM. In panel B, the sample was reduced by the addition of 2 mM sodium dithionite at room temperature for ~2 min before being frozen in liquid nitrogen. Conditions of measurements were as follows: microwave power, 1 mW; receiver gain, 2×10^4; modulation amplitude, 10 G; microwave frequency, 9.51 GHz.

species. Reduction of $RimO_{ai}$ with sodium dithionite results in the disappearance of this signal and the formation of a nearly axial EPR signal (0.22 equiv of spin) for which $g_{\|} \approx 2.06$ and $g_{\perp} \approx 1.94$ (Figure 2B, solid line). The intensity of this signal is significantly reduced with an increase in temperature to ~64 K (Figure 2B, dashed line). The observed *g* values of 2.06 and 1.94 and relaxation properties are typical of a $[4Fe\text{-}4S]^+$ cluster with an $S = {}^1/_2$ ground state. The additional feature at $g = 1.98$, which is also detectable at 64 K, is assigned to a small amount of $[2Fe\text{-}2S]^+$ clusters. This assignment is also corroborated by Mössbauer spectroscopy (vide infra).

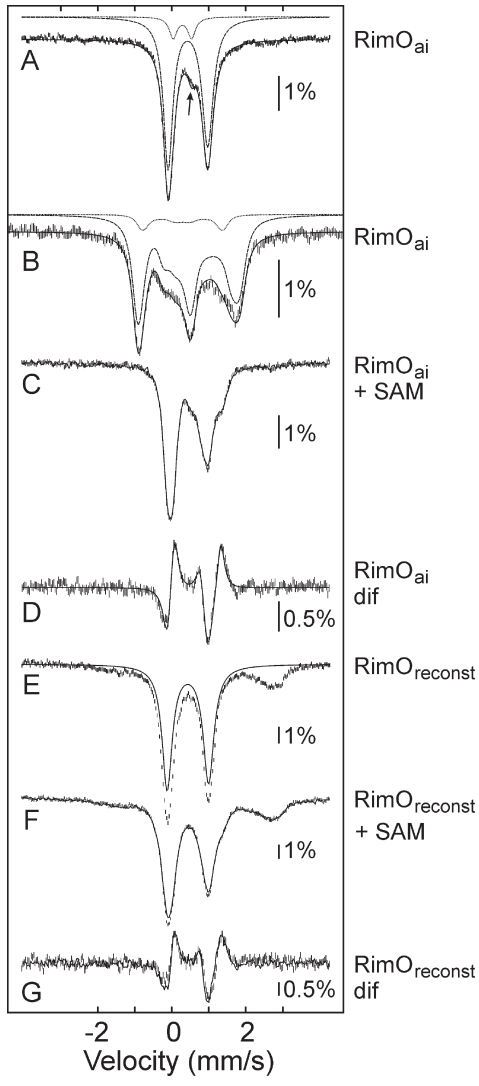

FIGURE 3: Mössbauer spectra (4.2 K) of RimO. All spectra were recorded in an external 53 mT magnetic field except for that in panel B, which was collected in a 6 T magnetic field oriented parallel to the γ-beam. (A) $RimO_{ai}$ (hash marks) and simulation with two quadrupole doublets (solid line) with the following parameters: $\delta_1 = 0.43$ mm/s, and $\Delta E_{Q,1} = 1.07$ mm/s (90% intensity); $\delta_2 = 0.29$ mm/s, and $\Delta E_{Q,2} = 0.49$ mm/s (10% intensity). The arrow is pointing to a line at ~0.5 mm/s. (B) $RimO_{ai}$ (hash marks) and spin Hamiltonian simulations (solid line) using the values for δ and ΔE_Q from panel A and the asymmetry parameters $\eta_1 = 0$ and $\eta_2 = 1$. (C) $RimO_{ai}$ in the presence of SAM (hash marks) and in the presence of SAM and **P1** (solid line). (D) Difference spectra between the hash mark spectra of panels A and C (hash marks) and simulation of the difference spectrum with three quadrupole doublets (solid line) with the following parameters: $\delta_1 = 0.43$ mm/s, and $\Delta E_{Q,1} = 1.07$ mm/s (32% downward); $\delta_2 = 0.70$ mm/s, and $\Delta E_{Q,2} = 1.24$ mm/s (16% upward); $\delta_3 = 0.37$ mm/s, and $\Delta E_{Q,3} = 0.81$ mm/s (16% upward). (E) $RimO_{rcn}$ (hash marks) and simulation of the $[4Fe\text{-}4S]^{2+}$ component with one quadrupole doublet (solid line) with the following parameters: $\delta_1 = 0.43$ mm/s, and $\Delta E_{Q,1} = 1.12$ mm/s (62% intensity). (F) $RimO_{ai}$ in the presence of SAM (hash marks) and in the presence of SAM and **P1** (solid line). (G) Comparison of the difference spectra obtained for binding of SAM in $RimO_{ai}$ and $RimO_{rcn}$. The hash marks correspond to the E − F difference spectrum and the solid line to the A − C difference spectrum. The concentrations of $RimO_{ai}$ and $RimO_{rcn}$ were 0.45 and 0.26 mM, respectively. SAM was used at a concentration of 3.5 mM. **P1** was used at a concentration of 3.7 mM.

Mössbauer spectroscopy was also used to determine the types and relative amounts of Fe-containing species in $RimO_{ai}$. The spectrum recorded at 4.2 K in a 53 mT external magnetic field (Figure 3A) is dominated by two intense lines emanating from a quadrupole doublet with parameters (isomer shift, δ, of 0.43 mm/s and quadrupole splitting, ΔE_Q, of 1.07 mm/s) typical of $[4Fe\text{-}4S]^{2+}$ clusters. In addition, there is a less intense line at ~0.5 mm/s indicated by an arrow. The position of this line is consistent with the high-energy line of the spectrum of $[2Fe\text{-}2S]^{2+}$ clusters. A simulation assuming two quadrupole doublets with the following parameters [$\delta_1 = 0.43$ mm/s, and $\Delta E_{Q,1} = 1.07$ mm/s (line widths $\Gamma_{left} = 0.30$ mm/s and $\Gamma_{right} = 0.36$ mm/s); $\delta_2 = 0.29$ mm/s, and $\Delta E_{Q,2} = 0.49$ mm/s ($\Gamma = 0.25$ mm/s)] is shown as a solid line overlaid with the data. The parameters corroborate the presence of $[4Fe\text{-}4S]^{2+}$ and $[2Fe\text{-}2S]^{2+}$ clusters at 90% total intensity and 10% total intensity, respectively. This assignment is further confirmed by a Mössbauer spectrum of $RimO_{ai}$ recorded in a 6 T external magnetic field (Figure 3B). The spectrum can be simulated with the parameters determined from the 53 mT spectrum (δ and ΔE_Q) and reveals that the magnetic field experienced by the ^{57}Fe nuclei equals the external magnetic field. This finding indicates that the internal magnetic field is zero and proves that the electronic ground state is diamagnetic ($S = 0$). Without exception, $[4Fe\text{-}4S]^{2+}$ and $[2Fe\text{-}2S]^{2+}$ clusters have diamagnetic ground states. Analytical and Mössbauer spectroscopy reveal that $RimO_{ai}$ harbors 4.0 (4.4 × 0.9) irons in the form of a [4Fe-4S] cluster, which amounts to 1.0 [4Fe-4S] cluster per $RimO_{ai}$ polypeptide. A significant fraction of the clusters on $RimO_{ai}$ are derived from the CxxxCxxC-coordinated RS [4Fe-4S] cluster, as indicated by perturbation of $RimO_{ai}$ upon addition of SAM (vide infra). The small amounts of the $[2Fe\text{-}2S]^{2+}$ cluster detected in this preparation of $RimO_{ai}$ are thought to result from partial degradation of the $[4Fe\text{-}4S]^{2+}$ cluster, which was previously observed for the RS enzyme pyruvate formate-lyase activating enzyme (*38*).

Spectroscopic and Analytical Characterization of Reconstituted RimO (*$RimO_{rcn}$*). $RimO_{ai}$ was reconstituted under anaerobic conditions with 8-fold molar excesses of ^{57}Fe and sodium sulfide in the presence of 10 mM DTT. The desalted protein sample had an intense brown color and was found to contain 11.4 ± 0.2 equiv of iron and 11.1 ± 0.7 equiv of sulfide per polypeptide chain using the Bradford correction factor. The UV−vis spectrum (Figure 1, dashed line) exhibited the same overall features observed in the spectrum of $RimO_{ai}$ but with increased intensity between 300 and 700 nm, resulting in an A_{280}/A_{410} ratio of 2.9. The 4.2 K, 53 mT Mössbauer spectrum of $RimO_{rcn}$ (Figure 3E, hash marks) is dominated by a quadrupole doublet with parameters indicative of $[4Fe\text{-}4S]^{2+}$ clusters: δ = 0.43 mm/s, and $\Delta E_Q = 1.12$ mm/s (62 ± 5% intensity). The presence of a broad and featureless absorption, which extends from approximately −3 to 3 mm/s,[2] results in the larger uncertainty for the absorption area of the quadrupole doublet associated with the $[4Fe\text{-}4S]^{2+}$ cluster. Analytical methods and Mössbauer analysis reveal that 7.1 ± 0.7 (11.4 × 0.62) irons are in the form of $[4Fe\text{-}4S]^{2+}$ clusters, corresponding to 1.8 ± 0.2 [4Fe-4S] clusters per polypeptide chain of $RimO_{rcn}$. We also characterized a second, independent sample of $RimO_{rcn}$ by the same methodology. The results reveal that this sample contained 14.9 Fe atoms per $RimO_{rcn}$, of which 55 ± 5% are in form of $[4Fe\text{-}4S]^{2+}$ clusters, as determined from the 4.2 K, 53 mT Mössbauer spectrum (Figure S3 of the Supporting Information). Thus, this sample exhibits a stoichiometry of 2.0 ± 0.2 [4Fe-4S] clusters per RimO. Taken together, these studies suggest the presence of two [4Fe-4S] clusters per RimO monomer, as suggested by bioinformatics and biochemical studies (*3*).

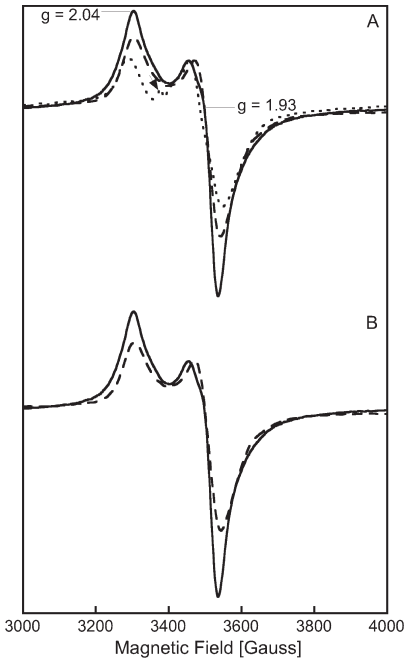

FIGURE 4: X-Band EPR spectra of (A) reduced $RimO_{rcn}$ (solid line), reduced $RimO_{ai}$ (dotted line), and reduced $RimO_{rcn}$ in the presence of SAM (dashed line) and (B) reduced $RimO_{rcn}$ (solid line) and reduced $RimO_{rcn}$ in the presence of SAM and **P1** (dashed line). The concentrations of $RimO_{ai}$ and $RimO_{rcn}$ were 0.45 and 0.26 mM, respectively. SAM was used at a concentration of 3.5 mM, while **P1** was used at a concentration of 3.7 mM. Each RimO sample was reduced by the addition of 2 mM sodium dithionite at room temperature for ~2 min before being frozen in liquid nitrogen. The solid line spectra in panels A and B display g values of ≈2.04 ($g_{\|}$) and ≈1.93 ($g_{\perp}$). The dashed line spectra in panels A and B display g values of ≈2.04 ($g_{\|}$) and ≈1.93 ($g_{\perp}$). The dotted line spectrum in panel A displays g values of ≈2.05 ($g_{\|}$) and ≈1.93 ($g_{\perp}$). In this same spectrum, the arrow is pointing to a $g \approx 2.0$ signal resulting from a cavity contaminant. Different scaling has been used for different spectra: ×1.0 for solid line spectra in panels A and B, ×5.0 for the dotted line spectrum in panel A, ×2.4 for the dashed line spectrum in panel A, and ×2.9 for the dashed line spectrum in panel B. Conditions of measurements were as follows: microwave power, 20 mW; temperature, 14 K; receiver gain, 2×10^4; modulation amplitude, 10 G; microwave frequency, 9.51 GHz.

The EPR spectrum of dithionite-reduced $RimO_{rcn}$ (0.29 equiv of spin) exhibits an axial EPR signal (Figure 4, solid line) with parameters typical of a $[4Fe\text{-}4S]^{+}$ cluster. The EPR spectrum is slightly perturbed compared to that of $RimO_{ai}$ (Figure 4A, dotted line), suggesting that the two clusters may have different EPR spectroscopic features. The absence of any other EPR-observable features in $RimO_{rcn}$ suggests that the aforementioned broad absorption in the Mössbauer spectrum is associated with unspecifically bound Fe, which is frequently observed in samples of Fe−S proteins that have been reconstituted with Fe^{2+}, Na_2S, and DTT (*21*).

[2]Accurate determination of the fraction associated with the $[4Fe\text{-}4S]^{2+}$ cluster subspectrum is important for the determination of the cluster stoichiometry. Therefore, we collected 4.2 K, 53 mT Mössbauer spectra over a wider range of Doppler velocities (±~12 mm/s, data not shown) to ensure that the unspecifically bound iron does not absorb outside the range of the spectra shown in Figure 3 (±~4 mm/s). Unspecifically bound iron does not absorb outside the ±~4 mm/s range of Doppler velocities.

*Effect of SAM and Peptide **P1** on the Mössbauer and EPR Spectra of RimO*. As shown in Figure 3C (hash marks), addition of the cosubstrate, SAM, to $RimO_{ai}$ perturbs the Mössbauer spectroscopic features of the $[4Fe\text{-}4S]^{2+}$ cluster(s) significantly. The difference spectrum (Figure 3D) between the hash mark spectra in panels A and C of Figure 3 can by simulated with three quadrupole doublets. The features pointing upward represent the Fe sites that are perturbed upon addition of SAM and are modeled by two quadrupole doublets of equal intensity with the following parameters: $\delta_1 = 0.70$ mm/s, and $\Delta E_{Q,1} = 1.24$ mm/s (16%); $\delta_2 = 0.37$ mm/s, and $\Delta E_{Q,2} = 0.81$ mm/s (16%). These two quadrupole doublets form at the expense of the quadrupole doublet pointing downward [$\delta = 0.43$ mm/s, and $\Delta E_Q = 1.07$ mm/s (32%)]. The Fe site with the increased isomer shift ($\delta = 0.70$ mm/s) is assigned to the unique, non-cysteinyl-coordinated Fe site of the CxxxCxxC-ligated RS [4Fe-4S] cluster. A comparably large isomer shift value of 0.72 was observed for the non-cysteinyl-coordinated Fe site in the RS enzyme pyruvate formate-lyase activating enzyme (PFL-AE) (*39*). The increased isomer shift is consistent with bidentate binding of SAM via its α-amino and carboxylate groups, which was observed for the SAM-bound form of PFL-AE (*40*). The isomer shift of the other site decreases from 0.43 to 0.37 mm/s. These spectroscopic changes (i.e., conversion of two Fe sites of a $[4Fe\text{-}4S]^{2+}$ cluster, of which one has an increased isomer shift and the other a decreased isomer shift) are remarkably similar to those observed for the $[4Fe\text{-}4S]^{2+}$ cluster of BS upon addition of SAM (*41*) and suggest that SAM binding to the unique site may perturb the electronic structure of the valence-delocalized $Fe_2^{2.5+}$ pair of the SAM-free form by localizing the extra electron more on the unique site [i.e., the unique site has more Fe(II) character, and the other site has more Fe(III) character]. Localization of the extra electron has also been observed for the $[4Fe\text{-}4S]^{2+}$ cluster of the non-RS enzyme ferredoxin:thioredoxin reductase (FTR), which is effected by coordination of the sulfur from C87, part of a disulfide bond, to one of the Fe sites (*42*). Addition of a 13-mer peptide, **P1** [which corresponds to the sequence surrounding the aspartate residue of S12 that becomes modified (residues 83−95)], to a solution of $RimO_{ai}$ and SAM does not result in additional perturbation of the Mössbauer spectrum (Figure 3C, solid line).

Addition of SAM to $RimO_{rcn}$ (Figure 3F, hash marks) results in spectroscopic perturbations (Figure 3G, hash marks) that are identical within experimental uncertainty to changes observed in the Mössbauer spectrum of $RimO_{ai}$ (Figure 3G, solid line). For $RimO_{rcn}$, 18% of the quadrupole doublet ($\delta = 0.43$ mm/s, and $\Delta E_Q = 1.07$ mm/s) is converted to 9% each of the quadrupole doublets with the following values upon addition of SAM: $\delta_1 = 0.70$ mm/s, $\Delta E_{Q,1} = 1.24$ mm/s, $\delta_2 = 0.37$ mm/s, and $\Delta E_{Q,2} = 0.81$ mm/s. The ratio of the absorption of the perturbed sites of the $[4Fe\text{-}4S]^{2+}$ cluster (18%) to the total absorption of the $[4Fe\text{-}4S]^{2+}$ clusters (62%) of 0.29 corresponds well with the interpretation given above that two of a total of eight Fe sites (from two [4Fe-4S] clusters) are perturbed. Addition of peptide **P1** does not yield additional perturbations (Figure 3F, solid line). Addition of SAM to a sample of reduced $RimO_{rcn}$ alters its EPR spectrum (0.22 equiv of spin) slightly as shown in Figure 4 (compare solid line to dashed line), which manifests itself primarily in the broadening of the $g = 2.04$ feature. This observation is consistent with the premise that SAM binds at or close to the cluster, which has been observed for a number of other RS enzymes (*33*, *39*−*41*, *43*). No additional effect is observed upon addition of **P1** to the $RimO_{rcn}$/SAM sample (Figure 4B, dashed line) (0.15 equiv of spin); the EPR spectrum of the $RimO_{rcn}$/SAM/**P1** sample is essentially indistinguishable from that of the $RimO_{rcn}$/SAM sample. The same behavior was observed for EPR spectra of $RimO_{ai}$, $RimO_{ai}$/SAM, and $RimO_{ai}$/SAM/**P1** samples (data not shown).

Activity Assay with $RimO_{rcn}$. Attempts to purify ribosomal protein S12, the native substrate for RimO, in soluble form were not successful. As a result, the MTTase activity of RimO was tested using peptide **P1** as a substrate analogue. Turnover was initially assessed by monitoring the production of 5′-dA and SAH as a function of time using an HPLC-based method with UV−vis detection. Dithionite was used as the requisite source of electrons in the assay. The generation of 5′-dA would signify a successful reductive cleavage of SAM, a step believed to be the first in the proposed mechanism of RimO (Scheme 2). Production of SAH would presumably indicate subsequent methyl transfer from a suggested second molecule of SAM to the proposed thiolated intermediate (Scheme 2). The time-dependent formation of 5′-dA [Figure 5 (●)] and SAH [Figure 5 (○)] in the reaction of $RimO_{rcn}$ in the presence of **P1** at 37 °C are both fitted to a first-order exponential equation with the following parameters: a rate constant (k) of 0.050 ± 0.001 min^{-1} and an amplitude (A) of 32.9 ± 0.4 μM for 5′-dA (Figure 5, solid line) and a k of 0.058 ± 0.006 min^{-1} and an A of 4.1 ± 0.1 μM for SAH (Figure 5, dashed line). The amplitudes from these fits reflect the maximal amount of respective product formed during the course of the reaction, implying that 0.33 equiv of 5′-dA and 0.04 equiv of SAH per $RimO_{rcn}$ are formed in vitro under the described conditions. In the absence of exogenous SAM, 0.03 equiv of 5′-dA is detected after 180 min, presumably from cleavage of tightly bound endogenous SAM,[3] while no SAH is observed. In the absence of **P1**, 0.05 equiv of SAH is detected, presumably formed as a result of nonproductive alkylation by the activated methyl group of SAM.

The 530 stem-loop of the 16S rRNA is in close proximity to residue D88 of the ribosomal S12 protein and is hypothesized to participate in binding to RimO during catalysis. To mimic the 530 stem-loop, we synthesized the 50 bp RNA oligomer corresponding to bases 498−547. Addition of this 50 bp oligomer at 175 μM to the described assay mixture results in time courses that are comparable to those observed in the absence of the RNA oligomer [Figure 5 (■ and □)]. This observation suggests that the designed 50 bp RNA oligomer is either not required or not suitable for recognition of the peptide by $RimO_{rcn}$, given that its presence does not augment the activity of the enzyme under the described conditions. An additional peptide, **P2** (RGGRVKALPGVRY), in which the aspartyl residue in peptide **P1** corresponding to D88 in protein S12 was changed to an alanyl residue, was also used as a substrate. As shown in Figure 5 (▲), peptide **P2** supports meager amounts of 5′-dA production, while the formation of SAH (0.06 equiv) is comparable to that in the presence of **P1** [Figure 5 (△)].

Detection of the Modified Product by Mass Spectrometry. Results from the HPLC-based kinetic assays imply that the reductive cleavage of SAM by $RimO_{rcn}$ to generate 5′-dA takes place in the presence of substrate analogue **P1**. However,

[3]The EPR and Mössbauer spectroscopic features of $RimO_{ai}$ are consistent with the presence of a small amount of the SAM-bound form, because the spectral features of the SAM-bound and SAM-free forms overlap heavily.

Scheme 2: Working Mechanistic Hypothesis for the Reaction Catalyzed by *E. coli* RimO[a]

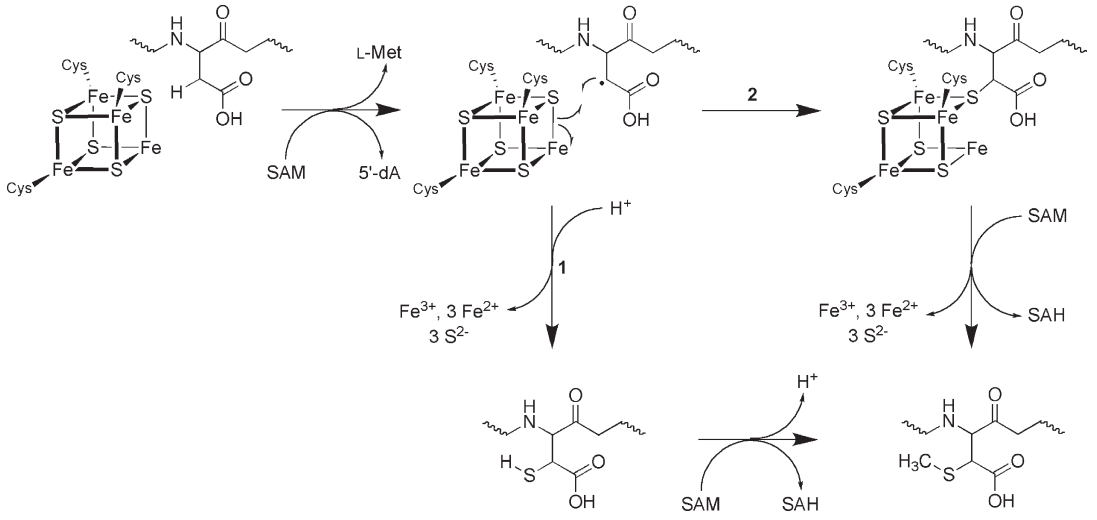

[a]The [4Fe-4S] cluster shown is that which is predicted to be coordinated by C17, C53, and C82. This cluster has an overall charge of +2, indicating the presence of formally two Fe^{3+} and two Fe^{2+} ions in its resting state. Two scenarios are shown for methylthiolation. In pathway 1, sulfur functionalization by a bridging μ-sulfido ligand of the cluster leads to cluster degradation. The resulting thiol-containing intermediate is methylated in a subsequent step that might potentially take place at a different location. In pathway 2, methylation of the attached sulfur atom takes place while it is still part of the Fe−S cluster, which subsequently leads to cluster degradation.

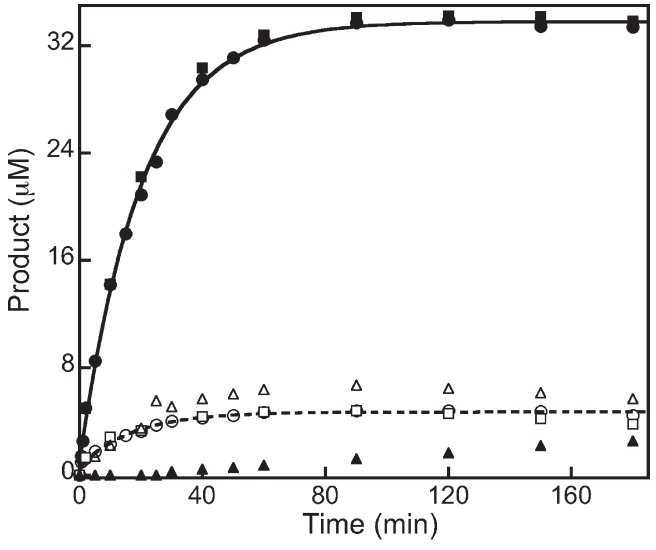

FIGURE 5: Time courses for the formation of 5′-dA and SAH in the reaction of $RimO_{rcn}$ with peptide substrate analogue **P1** or **P2** at 37 °C. Filled circles (●) describe formation of 5′-dA and empty circles (○) formation of SAH in the presence of **P1**. The solid and dashed lines are fits to a single first-order kinetic equation. The kinetic parameters obtained from these two fits are as follows: $A = 32.9 \pm 0.4\ \mu M$, $k = 0.050 \pm 0.001\ min^{-1}$, and $m = 0.91 \pm 0.29\ \mu M$ for formation of 5′-dA (—), and $A = 4.1 \pm 0.1\ \mu M$, $k = 0.058 \pm 0.006\ min^{-1}$, and $m = 0.63 \pm 0.12\ \mu M$ for formation of SAH (---), where A is the amplitude, k is the rate constant at 37 °C, and m is the intercept. Filled squares (■) describe the formation of 5′-dA and empty squares (□) the formation of SAH in the presence of **P1** and RNA oligo. Filled triangles (▲) describe the formation of 5′-dA and empty triangles (△) the formation of SAH in the presence of **P2**. The reaction was conducted as described in Materials and Methods, and the mixture contained 100 μM $RimO_{rcn}$, 700 μM SAM, 300 μM peptide, 50 mM Na-HEPES (pH 7.5), 2 mM dithionite, 1 mM tryptophan, and 175 μM RNA oligo where indicated.

the observation that comparable amounts of SAH are formed when either **P1** or **P2** is used as a substrate, or even in the complete absence of substrate, suggests that the production of SAH is not on the catalytic pathway, or that SAM is not the source of the methyl group in the SCH_3 modification. Effort, therefore, was focused on detection of the final product of the overall reaction, methylthiolated **P1**, by ESI-MS/MS. In the reaction of $RimO_{rcn}$ with **P1**, an m/z shift of +47 from the expected mass of **P1** is detected (Figure S4 of the Supporting Information), signifying the modification of **P1** by a methylthio group. The m/z value of 47 is one mass unit greater than expected; however, the ion trap mass spectrometer used has a mass resolution of ~1 Da under the conditions of data collection. As shown below, analysis of the peptide product by MALDI-TOF MS gave the expected m/z change of +46. The advantage in using the ion trap detector is that it allows the location of the modification to be determined (vide infra). Nonetheless, the intensity of the peak is estimated to be only 4% of that of the unmodified **P1** peak, indicating that very little methylthiolated **P1** is produced under the reaction conditions described. To ensure the authenticity of the m/z 47 peak, ESI-MS/MS spectra of the reactant and product peptides were generated (Figure 6). In the MS/MS spectrum of unmodified **P1** [m/z 369.2^{4+} (Figure 6B)], ions corresponding to b_6^{2+}, b_7^{2+}, and b_8^{2+} were detected. Similarly, the ion corresponding to b_6^{2+} was detected in the spectrum of modified **P1** [m/z 380.9^{4+} (Figure 6C)]; however, the b_7^{2+} and b_8^{2+} ions were now detected with a mass increase of 47 Da, equivalent to a modification of SCH_3 at residue 7 (Asp). These results confirm that the methylthio modification of **P1** by $RimO_{rcn}$ does indeed take place, specifically on the D88 residue. As a control, $RimO_{rcn}$ was incubated under turnover conditions with peptide **P2**, and the resulting peptides were analyzed by ESI-MS/MS for the modification. The fragment ion patterns for both samples, before and after reaction, were identical, indicating the lack of modification on peptide **P2**, which does not contain the relevant aspartyl residue (Figure S5 of the Supporting Information). Last, when the reaction was conducted with *S*-adenosyl-L-[*methyl*-d_3]methionine and then analyzed by MALDI-TOF MS, the product peptide displayed an m/z value of 1,522.00, 49 units greater than that of the substrate peptide

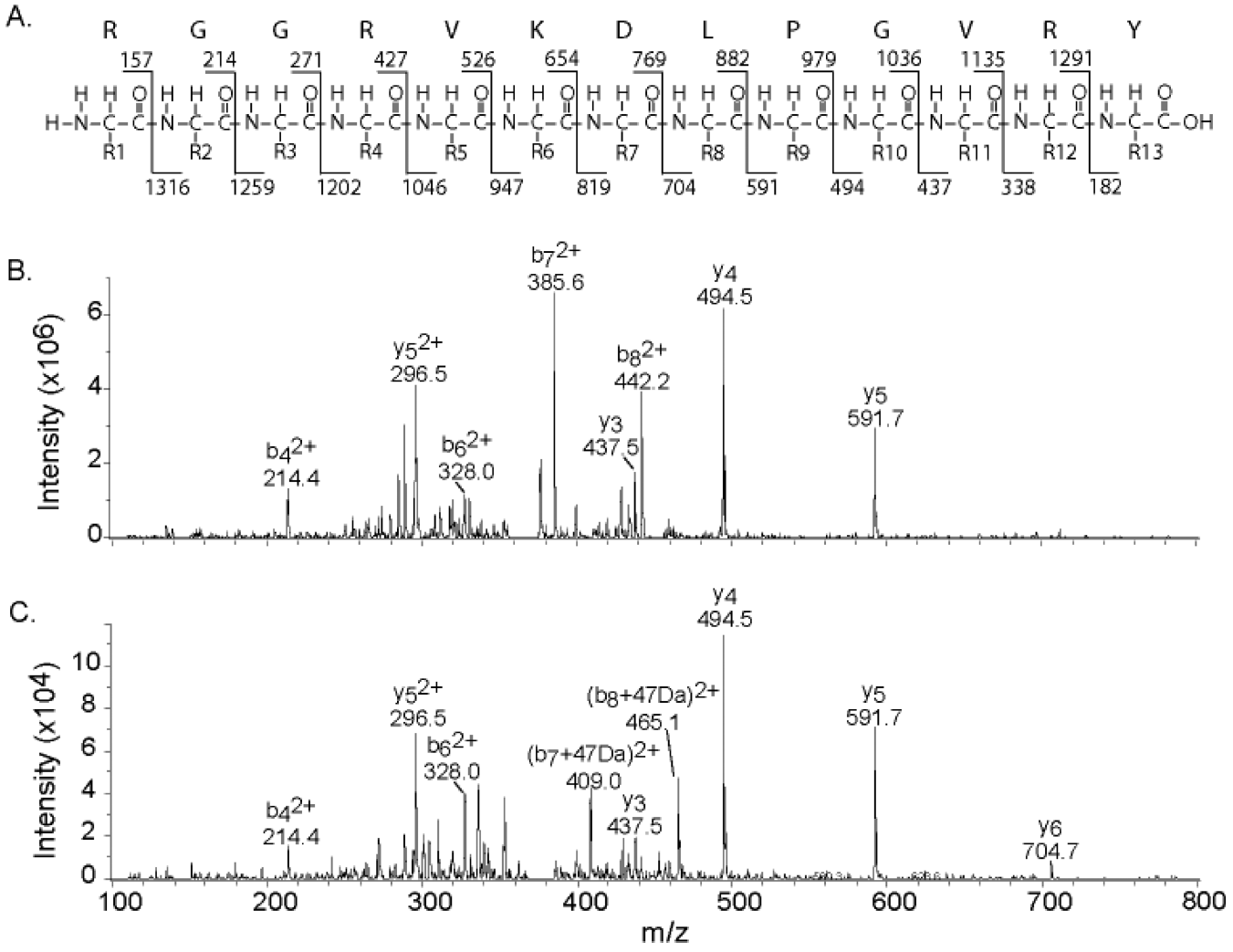

FIGURE 6: ESI-MS/MS spectra of the +4 ion of **P1**. (A) b and y fragment ions and their expected masses for **P1**. (B) Unmodified **P1** (*m*/*z* 369.17) at time zero. (C) Modified **P1** (*m*/*z* 380.9) at 15 min contains both the b_7^{2+} and b_8^{2+} +47 ions, indicative of methylthiolation on the Asp residue. The reaction mixture contained 100 μM $RimO_{rcn}$, 700 μM SAM, 300 μM **P1**, 50 mM Na-HEPES (pH 7.5), and 2 mM dithionite. Sample preparation is as discussed in Materials and Methods.

(*m*/*z* 1,472.99), consistent with removal of a hydrogen atom followed by the addition of a SCD_3 group (Figure S6 of the Supporting Information).

DISCUSSION

The ribosome is a complex machine, responsible for the careful decoding of mRNA and subsequent assembly of amino acids into discrete polypeptides. Bacterial ribosomes contain approximately 65% rRNA (rRNA) by weight, and indeed, it is the nucleic acids that are thought to contain the catalytic machinery necessary for formation of peptide bonds (*44*−*46*). However, rRNA is interspersed by a number of proteins that apparently assist in its proper folding and stabilization to ensure efficient decoding and assembly. Bacterial ribosomes can be separated easily into two unequal subunits that display sedimentation coefficients of 30S and 50S, a characteristic typically used to differentiate the two subunits. In *E. coli*, the 30S subunit is composed of 16S rRNA and 21 small proteins, labeled S1−S21, while the 50S subunit is composed of 5S and 23S rRNAs and 33 different proteins, labeled L1−L33 (*47*). A number of post-transcriptional modifications adorn rRNA, and some post-translational modifications, most often methylations, are found associated with various ribosomal proteins (*48*).

In 1977, Funatsu et al. reported the primary structure of protein S12 from *E. coli*, determined from peptide mapping and subsequent sequencing by Edman degradation, and noted that the amino acid at position 88 could not be assigned (*49*). Subsequent determination of the sequence of the gene that encodes protein S12 revealed the amino acid at position 88 to be an aspartyl residue (*50*). Almost 20 years later, analysis of protein S12 by MALDI-TOF MS revealed that it displayed a molecular mass of 13,652.0 Da, 46.1 Da larger than its gene sequence would predict (13,605.9 Da) (*1*). Further studies on peptides generated by enzymatic hydrolysis of protein S12 with trypsin revealed the modification to be associated with D88, and to be consistent with a thioether structure ($-SCH_3$) on the β-carbon, and inconsistent with a methylthiol structure ($-CH_2SH$) (*1*).

Bioinformatics and in vivo complementation studies have indicated that RimO, the product of the *yliG* gene in *E. coli*, is at least partly, if not fully, responsible for the introduction of a methylthio group at the β-carbon of D88 of protein S12 (*3*). This reaction is reminiscent of that catalyzed by MiaB, the final step in the biosynthesis of the hypermodified tRNA nucleoside ms^2i^6A, which is the methylthiolation of C^2 of adenine in the i^6A-37 intermediate (*4*, *20*). In the MiaB reaction, the hydrogen removed is nonacidic, limiting possibilities for formulation of

polar reaction mechanisms. Indeed, MiaB has been fairly well characterized (*20*, *22*) and is an accepted member of a special subclass of RS enzymes that catalyze the insertion or attachment of sulfur atoms at C−H bonds that are often completely unactivated (*15*). Others within this subclass that have been characterized include BS, which catalyzes the insertion of one sulfur atom between carbons 6 and 9 of dethiobiotin to afford biotin, and LS, which catalyzes two sulfur insertions at C6 and C8 of an octanoyl fatty amide chain appended to a lipoyl carrier protein (*17*−*19*).

One of the most salient characteristics of RS proteins that catalyze sulfur atom insertion is the observation that they, unlike most RS proteins, contain two Fe−S clusters. One cluster is housed in the canonical CxxxCxxC motif, or sometimes one that is slightly altered from the canonical sequence motif (*51*, *52*), while the other cluster is ligated by cysteines that occupy varying positions within the primary structure of the protein. In *E. coli* LS, this second cluster is a [4Fe-4S] cluster ligated by cysteinyl residues lying in a relatively compact motif, CxxxxCxxxxxC (*21*), while in MiaB from *E. coli*, the second cluster, also a [4Fe-4S] cluster, is ligated by C12, C49, and C83 (*22*). By contrast, the second Fe−S cluster in BS from *E. coli* is a [2Fe-2S] cluster ligated by C97, C128, C188, and R260 (*53*). Unlike the other amino acids that coordinate the [2Fe-2S] cluster, R260 appears to be a weak ligand, given that its substitution with several other amino acid residues does not significantly abrogate turnover by BS (*54*). In this work, we showed using Mössbauer spectroscopy in concert with quantitative analyses for iron and sulfide that RimO also contains two [4Fe-4S] clusters. $RimO_{ai}$, overproduced in *E. coli* containing an expression system for genes known to be involved in Fe−S cluster assembly in *A. vinelandii*, contained 4.4 ± 0.2 equiv of iron and 3.9 ± 0.4 equiv of sulfide per polypeptide, 90% of which was found by Mössbauer spectroscopy to be in the form of a $[4Fe\text{-}4S]^{2+}$ cluster and 10% of which was found to be in the form of a $[2Fe\text{-}2S]^{2+}$ cluster. Reconstitution of $RimO_{ai}$ with $^{57}FeSO_4$ and Na_2S, followed by gel filtration chromatography, led to a dramatic uptake of additional iron and sulfide, resulting in 11.4 ± 0.2 equiv of the former and 11.1 ± 0.7 equiv of the latter per polypeptide. However, analyses of the samples by Mössbauer spectroscopy showed that only 62 ± 5% of the iron was in the form of $[4Fe\text{-}4S]^{2+}$ clusters, while the remaining iron was nonspecifically bound. Mössbauer quantification allowed calculation of a resulting stoichiometry of 1.8 ± 0.2 $[4Fe\text{-}4S]^{2+}$ clusters per polypeptide, which is consistent with two [4Fe-4S] clusters per polypeptide. A second determination of cluster stoichiometry on a different batch of $RimO_{rcn}$ gave 2.0 ± 0.2 $[4Fe\text{-}4S]^{2+}$ clusters per polypeptide.

The number of cysteinyl residues on *E. coli* RimO is nine; however, a sequence alignment of RimO proteins from four different species, including *E. coli*, *Aquifex aeolicus*, *Pasteurella multocida*, and *Synechocystis* sp. (strain PCC 6803), indicates that only six cysteinyl residues are absolutely conserved, consistent with what is found in other proteins that catalyze sulfur insertion or methylthiolation reactions, all of which have two Fe−S clusters per polypeptide (*15*). In *E. coli* RimO, three of the conserved cysteinyl residues lie in the canonical RS CxxxCxxC motif, while the remaining three, C17, C53, and C82, reside in the N-terminal half of the protein, as found in MiaB. Moreover, the spacing between the cysteinyl residues is similar, though not exact, in both proteins. As we will describe below, we posit that the Fe−S cluster predicted to be ligated by C17, C53, and C82 is the source of the sulfur incorporated into the substrate, and that it is sacrificed during turnover, as postulated for BS, LS, and MiaB (*15*, *20*−*22*, *24*).

The substrate for RimO is a 13.7 kDa protein, ribosomal protein S12, which binds to 16S rRNA and makes minor contacts with ribosomal proteins S8 and S17 (*2*). Currently, it is not known whether RimO modifies protein S12 in an unfolded state, a folded state, or a completely assembled ribosome. The observation that RimO contains a TRAM domain, a motif shown to be involved in RNA binding in other proteins, would suggest the latter; however, it is conceivable that the TRAM domain might recognize a polypeptide structural motif that mimics partially folded RNA. Initial efforts to overproduce a hexahistidine-tagged form of protein S12 were unsuccessful; the protein was found almost exclusively as insoluble aggregates. Therefore, turnover was assessed in the presence of a peptide, **P1**, that corresponds to residues 83−95 of the *E. coli* S12 protein. This peptide triggered reductive cleavage of SAM, which proceeded with pseudo-first-order kinetic behavior, resulting in formation of ~0.3 equiv of 5′-dA per polypeptide after incubation for 1 h at 37 °C. Importantly, very little formation of 5′-dA was observed after incubation for 3 h at 37 °C in the absence of peptide **P1** (≤0.002 equiv) or in the presence of peptide **P2** (< 0.03 equiv), in which the residue corresponding to D88 was changed to alanyl.

On the basis of similarities with the proposed MiaB reaction, the other SAM-related product of the RimO reaction is expected to be SAH, formed via a subsequent SAM-dependent methyltransferase reaction (*20*). Formation of SAH was indeed observed, albeit in meager amounts, and not stoichiometric with protein and 5′-dA. Nevertheless, the amount of SAH formed after incubation for 3 h at 37 °C (~4 μM) was on par with the amount of methylthiolated peptide **P1** as estimated from analysis by mass spectrometry (~12 μM). It is expected that RimO should produce no more than 1 equiv of methylthiolated product per equivalent of enzyme, given that an Fe−S cluster on the protein is expected to be the source of the inserted sulfur atom. The low extent of full turnover is possibly related to the employment of an unnatural substrate in the reaction. Although 5′-dA was generated in respectable amounts, there was no evidence from analysis by mass spectrometry of production of a thiolated species, although more detailed studies are needed to assess the involvement of this presumed intermediate. Perplexingly, SAH was formed in comparable amounts under conditions in which 5′-dA was not, as in the absence of a peptide substrate, or in the presence of peptide **P2**. Moreover, its formation under all conditions was enzyme-dependent, followed pseudo-first-order kinetic behavior, and displayed a rate constant that was on par with that for formation of 5′-dA, characteristics that are consistent with its relevance in catalysis. The obvious question, therefore, is the nature of the species that becomes methylated in the absence of substrate. As described below, we speculate that this species might be one of the bridging μ-sulfido ligands of the sacrificed [4Fe-4S] cluster.

Although the order of thiolation and methylation has not been elucidated for either MiaB or RimO in vitro, previous in vivo evidence hints that thiolation precedes methylation in MiaB. Starvation of an *E. coli* (*rel met cys*) mutant with methionine but not cysteine resulted in the trapping of a cytokinin active intermediate suspected to be 2-thio-N^6-(Δ^2-isopentenyl)adenosine (s^2i^6A). Incubation of this intermediate with *E. coli* crude extract and [*methyl*-^{14}C]SAM under aerobic conditions resulted in incorporation of the radiolabel (*55*). Furthermore, the cysteine/sulfate-deficient mutant resulted in accumulation of i^6A that was unreactive toward methylation under the same

experimental conditions, suggesting that methylation by MiaB, and probably other MTTases, including RimO, relies on prior sulfur insertion by an active Fe−S cluster.

Inspection of the amino acid sequences of both RimO and MiaB shows no evidence of known SAM binding motifs that are generally present in most methyltransferases (MTases) (*3*). However, thiopurine MTase, a SAM-dependent MTase that methylates purine sulfur substituents, also lacks any conserved motifs despite adopting a classical SAM-dependent MTase fold (*56*). Therefore, it is expected that residues involved in binding the second SAM molecule are contained within the N-terminal or RS domain and are conserved among different MTTases. The exclusion of the TRAM domain as a possible SAM binding domain stems from the observation that methyl transfer in protein RumA is conducted by a dedicated SAM binding motif that is distinct from the TRAM domain (*9*).

In Scheme 2, we provide a mechanistic working hypothesis for RimO-catalyzed methylthiolation of D88 of protein S12, which is analogous to one described for MiaB (*20*). In this mechanism, SAM, which presumably coordinates to the non-cysteinyl-ligated Fe of the RS [4Fe-4S] cluster, is reductively cleaved to generate a 5′-dA$^{\bullet}$. The 5′-dA$^{\bullet}$ abstracts a hydrogen atom from C_{β} of D88, generating a substrate radical that attacks a bridging μ-sulfido ligand of the non-RS [4Fe-4S] cluster with concomitant inner-sphere electron transfer to—formally—an Fe^{3+} ion in the cluster to afford an Fe^{2+} ion. The resulting cluster may then decompose, allowing release of a thiolated intermediate, which might undergo further methylation at that site or at a different site on the protein (Scheme 2, pathway 1). Alternatively, methylation of the thiolated species might proceed while the sulfur remains as a constituent of the Fe−S cluster (Scheme 2, pathway 2). At present, we prefer the latter scenario for the following reason. All RS enzymes that catalyze sulfur insertion using an Fe−S cluster as the source of the sulfur atom, four that have been studied in vitro, do so in two discrete half-reactions, with two potential insults to the relevant Fe−S cluster. For example, formation of the thiophane ring of biotin requires an attack of two different substrate radicals on a bridging μ-sulfido atom of a [2Fe-2S] cluster, while the formation of lipoic acid presumably requires an attack of two different substrate radicals on two different sulfur atoms in the same [4Fe-4S] cluster (*15*). In fact, evidence suggests that the presumed monothiolated intermediate in the LS reaction is tightly bound, consistent with breakdown of the [4Fe-4S] cluster only after the second sulfur insertion (*57*, *58*). In methylthiolation reactions, such as those catalyzed by RimO and MiaB, the second insult to the cluster, initiating its decomposition and allowing for product release, could be methylation of the inserted sulfur atom while it remains a constituent of the Fe−S cluster. A third mechanism, which is also consistent with our observations, could involve initial methylation of a bridging μ-sulfido ligand of the cluster, with subsequent transfer of the methythiol group as one unit using RS machinery.

The stereochemical course of sulfur insertion or addition in this subclass of RS enzymes varies. In BS, the C6 *pro-S* hydrogen is abstracted by the 5′-dA$^{\bullet}$, and sulfur insertion takes place with retention of configuration (*59*, *60*). By contrast, in LS, the C6 *pro-R* hydrogen is abstracted by the 5′-dA$^{\bullet}$, but sulfur insertion takes place with inversion of configuration (*60*). In MiaB, a hydrogen atom is abstracted from an sp^2-hybridized carbon. In the case of RimO, although the β-carbon of an aspartyl residue is prochiral, it has not been determined which hydrogen (*pro-S* or *pro-R*) is removed during turnover. In fact, the stereochemical configuration of methylthiolated D88 is unknown.

In summary, we have cloned the *yliG* gene from *E. coli* and have shown that its product, RimO, contains two [4Fe-4S] clusters. One of these clusters is presumed to be ligated by C150, C154, and C157, found in a canonical RS signature motif, while the other is predicted to be ligated by C17, C53, and C82, found near the N-terminus of the protein. Although the post-translational modification takes place on a 13.7 kDa protein, we showed that a 13-amino acid synthetic peptide, corresponding to residues 83−95 of protein S12 from *E. coli*, supports at least partial turnover. One point of significant importance that remains to be elucidated is the detailed mechanism of the reaction, especially as it pertains to any intermediates that involve the cluster presumed to be sacrificed during turnover, as well as the mechanism and timing of methyl transfer.

ACKNOWLEDGMENT

We thank Professor Catherine L. Drennan and her group (Department of Chemistry, Massachusetts Institute of Technology, Cambridge, MA) for allowing us the use of their anaerobic facility. We thank Tyler L. Grove (Department of Chemistry, Pennsylvania State University, University Park, PA) for assistance in verifying production of SAH and 5′-dA by mass spectrometry as well as help with MALDI-TOF MS.

SUPPORTING INFORMATION AVAILABLE

Figures S1−S6. This material is available free of charge via the Internet at http://pubs.acs.org.

REFERENCES

1. Kowalak, J. A., and Walsh, K. A. (1996) β-Methylthio-aspartic acid: Identification of a novel posttranslational modification in ribosomal protein S12 from *Escherichia coli*. *Protein Sci. 5*, 1625–1632.
2. Brodersen, D. E., Clemons, W. M., Jr., Carter, A. P., Wimberly, B. T., and Ramakrishnan, V. (2002) Crystal structure of the 30 S ribosomal subunit from *Thermus thermophilus*: Structure of the proteins and their interactions with 16S RNA. *J. Mol. Biol. 316*, 725–768.
3. Anton, B. P., Saleh, L., Benner, J. S., Raleigh, E. A., Kasif, S., and Roberts, R. J. (2008) RimO, a MiaB-like enzyme, methylthiolates the universally conserved Asp88 residue of ribosomal protein S12 in *Escherichia coli*. *Proc. Natl. Acad. Sci. U.S.A. 105*, 1826–1831.
4. Esberg, B., Leung, H.-C. E., Tsui, H.-C. T., Björk, G. R., and Winkler, M. E. (1999) Identification of the *miaB* gene, involved in methylthiolation of isopentenylated A37 derivatives in the tRNA of *Salmonella typhimurium* and *Escherichia coli*. *J. Bacteriol. 181*, 7256–7265.
5. Pierrel, F., Björk, G. R., Fontecave, M., and Atta, M. (2002) Enzymatic modification of tRNAs: MiaB is an iron−sulfur protein. *J. Biol. Chem. 277*, 13367–13370.
6. Pierrel, F., Hernández, H. L., Johnson, M. K., Fontecave, M., and Atta, M. (2003) Characterization of an extremely thermophilic tRNA-methylthiotransferase. *J. Biol. Chem. 278*, 29515–29524.
7. Kaminska, K. H., Baraniak, U., Boniecki, M., Nowaczyk, K., Czerwoniec, A., and Bujnicki, J. M. (2007) Structural bioinformatics analysis of enzymes involved in the biosynthesis pathway of the hypermodified nucleoside ms^2io^6A37 in tRNA. *Proteins 70*, 1–18.
8. Anantharaman, V., Koonin, E. V., and Aravind, L. (2001) TRAM, a predicted RNA-binding domain, common to tRNA uracil methylation and adenine thiolation enzymes. *FEMS Microbiol. Lett. 197*, 215–221.
9. Lee, T. T., Agarwalla, S., and Stroud, R. M. (2004) Crystal structure of RumA, an iron-sulfur cluster containing *E. coli* ribosomal RNA 5-methyluridine methyltransferase. *Structure 12*, 397–407.
10. Lee, T. T., Agarwalla, S., and Stroud, R. M. (2005) A unique RNA fold in the RumA-RNA-cofactor ternary complex contributes to substrate selectivity and enzymatic function. *Cell 120*, 599–611.
11. Nissen, P., Kjeldgaard, M., Thirup, S., Polekhina, G., Reshetnikova, L., Clark, B. F., and Nyborg, J. (1995) Crystal structure of the ternary complex of Phe-tRNAPhe, EF-Tu, and a GTP analog. *Science 270*, 1464–1472.

12. Selmer, M., Al-Karadaghi, S., Hirokawa, G., Kaji, A., and Liljas, A. (1999) Crystal structure of *Thermotoga maritima* ribosome recycling factor: A tRNA mimic. *Science 286*, 2349–2352.
13. Alexander, R. W., Muralikrishna, P., and Cooperman, B. S. (1994) Ribosomal components neighboring the conserved 518−533 loop of 16S rRNA in 30S subunits. *Biochemistry 33*, 12109–12118.
14. Stern, S., Powers, T., Changchien, L. M., and Noller, H. F. (1988) Interaction of ribosomal proteins S5, S6, S11, S12, S18 and S21 with 16S rRNA. *J. Mol. Biol. 201*, 683–695.
15. Booker, S. J., Cicchillo, R. M., and Grove, T. L. (2007) Self-sacrifice in radical S-adenosylmethionine proteins. *Curr. Opin. Chem. Biol. 11*, 543–552.
16. Sanyal, I., Cohen, G., and Flint, D. H. (1994) Biotin synthase: Purification, characterization as a [2Fe-2S] cluster protein, and in vitro activity of the *Escherichia coli bioB* gene product. *Biochemistry 33*, 3625–3631.
17. Cicchillo, R. M., Iwig, D. F., Jones, A. D., Nesbitt, N. M., Baleanu-Gogonea, C., Souder, M. G., Tu, L., and Booker, S. J. (2004) Lipoyl synthase requires two equivalents of S-adenosyl-L-methionine to synthesize one equivalent of lipoic acid. *Biochemistry 43*, 6378–6386.
18. Zhao, S., Miller, J. R., Jiang, Y., Marletta, M. A., and Cronan, J. E., Jr. (2003) Assembly of the covalent linkage between lipoic acid and its cognate enzymes. *Chem. Biol. 10*, 1293–1302.
19. Miller, J. R., Busby, R. W., Jordan, S. W., Cheek, J., Henshaw, T. F., Ashley, G. W., Broderick, J. B., Cronan, J. E., Jr., and Marletta, M. A. (2000) *Escherichia coli* LipA is a lipoyl synthase: In vitro biosynthesis of lipoylated pyruvate dehydrogenase complex from octanoyl-acyl carrier protein. *Biochemistry 39*, 15166–15178.
20. Pierrel, F., Douki, T., Fontecave, M., and Atta, M. (2004) MiaB protein is a bifunctional radical-S-adenosylmethionine enzyme involved in thiolation and methylation of tRNA. *J. Biol. Chem. 279*, 47555–47653.
21. Cicchillo, R. M., Lee, K.-H., Baleanu-Gogonea, C., Nesbitt, N. M., Krebs, C., and Booker, S. J. (2004) *Escherichia coli* lipoyl synthase binds two distinct [4Fe-4S] clusters per polypeptide. *Biochemistry 43*, 11770–11781.
22. Hernández, H. L., Pierrel, F., Elleingand, E., García-Serres, R., Huynh, B. H., Johnson, M. K., Fontecave, M., and Atta, M. (2007) MiaB, a bifunctional radical-S-adenosylmethionine enzyme involved in the thiolation and methylation of tRNA, contains two essential [4Fe-4S] clusters. *Biochemistry 46*, 5140–5147.
23. Cosper, M. M., Jameson, G. N. L., Hernández, H. L., Krebs, C., Huynh, B. H., and Johnson, M. K. (2004) Characterization of the cofactor composition of *Escherichia coli* biotin synthase. *Biochemistry 43*, 2007–2021.
24. Ugulava, N. B., Sacanell, C. J., and Jarrett, J. T. (2001) Spectroscopic changes during a single turnover of biotin synthase: Destruction of a [2Fe-2S] cluster accompanies sulfur insertion. *Biochemistry 40*, 8352–8358.
25. Ugulava, N. B., Surerus, K. K., and Jarrett, J. T. (2002) Evidence from Mössbauer sectroscopy for distinct $[2Fe\text{-}2S]^{2+}$ and $[4Fe\text{-}4S]^{2+}$ cluster binding sites in biotin synthase from *Escherichia coli*. *J. Am. Chem. Soc. 124*, 9050–9051.
26. Iwig, D. F., and Booker, S. J. (2004) Insight into the polar reactivity of the onium chalcogen analogues of S-adenosyl-L-methionine. *Biochemistry 43*, 13496–13509.
27. Bradford, M. (1976) A rapid and sensitive method for the quantitation of microgram quantities of protein utilizing the principle of protein dye binding. *Anal. Biochem. 72*, 248–254.
28. Beinert, H. (1978) Micro methods for the quantitative determination of iron and copper in biological material. *Methods Enzymol. 54*, 435–445.
29. Beinert, H. (1983) Semi-micro methods for analysis of labile sulfide and of labile sulfide plus sulfane sulfur in unusually stable iron-sulfur proteins. *Anal. Biochem. 131*, 373–378.
30. Kennedy, M. C., Kent, T. A., Emptage, M., Merkle, H., Beinert, H., and Münck, E. (1984) Evidence for the formation of a linear [3Fe-4S] cluster in partially unfolded aconitase. *J. Biol. Chem. 259*, 14463–14471.
31. Grove, T. L., Lee, K.-H., St. Clair, J., Krebs, C., and Booker, S. J. (2008) In vitro characterization of AtsB, a radical SAM formylglycine-generating enzyme that contains three [4Fe-4S] clusters. *Biochemistry 47*, 7523–7538.
32. Sofia, H. J., Chen, G., Hetzler, B. G., Reyes-Spindola, J. F., and Miller, N. E. (2001) Radical SAM, a novel protein superfamily linking unresolved steps in familiar biosynthetic pathways with radical mechanisms: Functional characterization using new analysis and information visualization methods. *Nucleic Acids Res. 29*, 1097–1106.
33. Cheek, J., and Broderick, J. B. (2001) Adenosylmethionine-dependent iron-sulfur enzymes: Versatile clusters in a radical new role. *J. Biol. Inorg. Chem. 6*, 209–226.
34. Fontecave, M., Mulliez, E., and Ollagnier, S. (2001) Adenosylmethionine as a source of 5′-deoxyadenosyl radicals. *Curr. Opin. Chem. Biol. 5*, 506–511.
35. Frey, P. A., and Booker, S. J. (2001) Radical mechanisms of S-adenosylmethionine-dependent enzymes. *Adv. Protein Chem. 58*, 1–45.
36. Frey, P. A., and Magnusson, O. T. (2003) S-Adenosylmethionine: A wolf in sheep's clothing, or a rich man's adenosylcobalamin? *Chem. Rev. 103*, 2129–2148.
37. Johnson, D. C., Unciuleac, M. C., and Dean, D. R. (2006) Controlled expression and functional analysis of iron-sulfur cluster biosynthetic components within *Azotobacter vinelandii*. *J. Bacteriol. 188*, 7551–7561.
38. Krebs, C., Henshaw, T. F., Cheek, J., Huynh, B. H., and Broderick, J. B. (2000) Conversion of 3Fe-4S to 4Fe-4S clusters in native pyruvate formate-lyase activating enzyme: Mössbauer characterization and implications for mechanism. *J. Am. Chem. Soc. 122*, 12497–12506.
39. Krebs, C., Broderick, W. E., Henshaw, T. F., Broderick, J. B., and Huynh, B. H. (2002) Coordination of adenosylmethionine to a unique iron site of the [4Fe-4S] of pyruvate formate-lyase activating enzyme: A Mössbauer spectroscopic study. *J. Am. Chem. Soc. 124*, 912–913.
40. Walsby, C. J., Ortillo, D., Yang, J., Nnyepi, M. R., Broderick, W. E., Hoffman, B. M., and Broderick, J. B. (2005) Spectroscopic approaches to elucidating novel iron-sulfur chemistry in the "radical-SAM" protein superfamily. *Inorg. Chem. 44*, 727–741.
41. Cosper, M. M., Jameson, G. N. L., Davydov, R., Eidsness, M. K., Hoffman, B. M., Huynh, B. H., and Johnson, M. K. (2002) The $[4Fe\text{-}4S]^{2+}$ cluster in reconstituted biotin synthase binds S-adenosyl-L-methionine. *J. Am. Chem. Soc. 124*, 14006–14007.
42. Walters, E. M., García-Serres, R., Jameson, G. N. L., Glauser, D. A., Bourgquin, F., Manieri, W., Schürmann, P., Johnson, M. K., and Huynh, B. H. (2005) Spectroscopic characterization of site-specific $[Fe_4S_4]$ cluster chemistry in ferredoxin:thioredoxin reductase: Implications for the catalytic mechanism. *J. Am. Chem. Soc. 127*, 9612–9624.
43. Layer, G., Heinz, D. W., Jahn, D., and Schubert, W. D. (2004) Structure and function of radical SAM enzymes. *Curr. Opin. Chem. Biol. 8*, 468–476.
44. Ban, N., Nissen, P., Hansen, J., Moore, P. B., and Steitz, T. A. (2000) The complete atomic structure of the large ribosomal subunit at 2.4 Å resolution. *Science 289*, 905–920.
45. Carter, A. P., Clemons, W. M., Brodersen, D. E., Morgan-Warren, R. J., Wimberly, B. T., and Ramakrishnan, V. (2000) Functional insights from the structure of the 30S ribosomal subunit and its interactions with antibiotics. *Nature 407*, 340–348.
46. Noller, H. F., Hoffarth, V., and Zimniak, L. (1992) Unusual resistance of peptidyl transferase to protein extraction procedures. *Science 256*, 1416–1419.
47. Nelson, D. L., and Cox, M. M. (2008) Lehninger, Principles of Biochemistry , 5th ed., W. H. Freeman and Co., New York.
48. Arnold, R. J., and Reilly, J. P. (1999) Observation of *Escherichia coli* ribosomal proteins and their posttranslational modifications by mass spectrometry. *Anal. Biochem. 269*, 105–112.
49. Funatsu, G., Yaguchi, M., and Wittmann-Liebold, B. (1977) Primary structure of protein S12 from the small *Escherichia coli* ribosomal subunit. *FEBS Lett. 73*, 12–17.
50. Post, L. E., and Nomura, M. (1980) DNA sequences from the *str* operon of *Escherichia coli*. *J. Biol. Chem. 255*, 4660–4666.
51. Chatterjee, A., Li, Y., Zhang, Y., Grove, T. L., Lee, M., Krebs, C., Booker, S. J., Begley, T. P., and Ealick, S. E. (2008) Reconstitution of ThiC in thiamine pyrimidine biosynthesis expands the radical SAM superfamily. *Nat. Chem. Biol. 4*, 758–765.
52. Martinez-Gomez, N. C., and Downs, D. M. (2008) ThiC is an [Fe-S] cluster protein that requires AdoMet to generate the 4-amino-5-hydroxymethyl-2-methylpyrimidine moiety in thiamin synthesis. *Biochemistry 47*, 9054–9056.
53. Berkovitch, F., Nicolet, Y., Wan, J. T., Jarrett, J. T., and Drennan, C. L. (2004) Crystal structure of biotin synthase, an S-adenosylmethionine-dependent radical enzyme. *Science 303*, 76–79.
54. Broach, R. B., and Jarrett, J. T. (2006) Role of the $[2Fe\text{-}2S]^{2+}$ cluster in biotin synthase: Mutagenesis of the atypical metal ligand arginine 260. *Biochemistry 45*, 14166–14174.
55. Agris, P. F., Armstrong, D. J., Schäfer, K. P., and Söll, D. (1975) Maturation of a hypermodified nucleoside in transfer RNA. *Nucleic Acids Res. 2*, 691–698.

56. Scheuermann, T. H., Lolis, E., and Hodsdon, M. E. (2003) Tertiary structure of thiopurine methyltransferase from *Pseudomonas syringae*, a bacterial orthologue of a polymorphic, drug-metabolizing enzyme. *J. Mol. Biol. 333*, 573–585.
57. Cicchillo, R. M., and Booker, S. J. (2005) Mechanistic investigations of lipoic acid biosynthesis in *Escherichia coli*: Both sulfur atoms in lipoic acid are contributed by the same lipoyl synthase polypeptide. *J. Am. Chem. Soc. 127*, 2860–2861.
58. Douglas, P., Kriek, M., Bryant, P., and Roach, P. L. (2006) Lipoyl synthase inserts sulfur atoms into an octanoyl substrate in a stepwise manner. *Angew. Chem. 118*, 5321–5323.
59. Marquet, A., Tse Sum Bui, B., and Florentin, D. (2001) Biosynthesis of biotin and lipoic acid. *Vitam. Horm. 61*, 51–101.
60. Parry, R. J. (1983) Biosynthesis of some sulfur-containing natural products. Investigations of the mechanism of carbon-sulfur bond formation. *Tetrahedron 39*, 1215–1238.